

Metallicity relations in LMC and SMC from the slope of Red Giant Branch stars in globular clusters.

Saurabh Sharma^{1*} and Jura Borissova²

^{1*}Aryabhata Research Institute of Observational Sciences (ARIES), Manora Peak, Nainital, 263 001, India.

²Instituto de Física y Astronomía, Universidad de Valparaíso, Ave. Gran Bretaña 1111, Valparaíso, Chile; Millennium Institute of Astrophysics, MAS, Chile.

*Corresponding author(s). E-mail(s): saurabh@aries.res.in;

Contributing authors: jura.borissova@uv.cl;

Abstract

Red giants are an excellent tool for probing the history of star formation and subsequent metallicity evolution in the galaxies. The well-defined red giant branch (RGB) stars of the globular clusters can be used to determine their slopes and to calibrate the RGB slope parameters, age, and metallicity relations. We obtained deep near-IR *JHK* stellar photometry of 23 LMC/SMC globular clusters. The cluster sample covers a wide range in metallicities ($-1.76 < [\text{Fe}/\text{H}] < -0.32$) and ages ($0.6 \text{ Gyr} < t < 14 \text{ Gyr}$). The slope of the RGBs of each cluster was calculated and used to derive the relations between slope-age-metallicity. We have found that the RGB slope do not shows any statistically significant age dependence. The young and old clusters are found to be distributed differently in RGB slope-metallicity space, and the younger populations show a slightly less steep RGB slope dependence than the whole cluster sample. The population of the younger clusters shows a negative slope, whereas the older clusters show a positive slope.

Keywords: Hertzsprung-Russel (HR) diagram – globular clusters: general – galaxies: abundances – galaxies: individual (LMC, SMC) – infrared: stars

1 Introduction

Red giant branch (RGB) stars are among the brightest red stars in stellar systems older than a Gyr. They appear in essentially all galaxies. Therefore, red giants are an excellent tool for probing the parameters of old populations and the history of star formation in galaxies. Globular clusters, on the other hand, are ideal sites for calibrating the RGB parameters. Since [Da Costa & Hatzidimitroui 1998] explored the possibility of using the position of the RGB as a metallicity indicator, many significant

advances have been made in improving astronomical instrumentation and developing the corresponding theory. The infrared (IR) wavelength regime became accessible, and it is particularly compelling for such studies, in comparison with the optical one, because of the potential to probe the stellar populations of systems with high intrinsic extinction. Aside from minimizing reddening effects, the near-IR spectral region “straightens” the RGB, converting it from a hyperbola (as seen in [Saviane et al. 2000]) to a straight line ([Ivanov & Borissova 2002]). This implies that the

depth of the photometry is not as crucial in the near-IR as in the optical to establish a slope. Red giants are brighter in the IR, and the RGB slope is independent of distance and reddening. Also, the IR can help break the age-metallicity degeneracy that plagues the optical.

[Kuchinski et al. 1995] and [Minniti et al. 1995] demonstrated both empirically and theoretically that the slope of the RGB in a K vs. $(J - K)$ color-magnitude diagram (CMD) is sensitive to the metallicity of the population. They investigated this correlation for metal-rich globular clusters and derived a linear relation between $[\text{Fe}/\text{H}]$ and RGB slope. [Ivanov et al. 2000] extended this relation to metallicities as low as $[\text{Fe}/\text{H}] = -2.1$. [Ferraro et al. 2000] used high-quality data for ten Galactic globular clusters and derived a similar relation. [Ivanov & Borissova 2002] tabulated the relation in $[M_K, (J - K_S), [\text{Fe}/\text{H}]$ space based on a large sample of 2MASS photometry of Milky Way globular clusters. They fitted straight lines to the RGBs stars and produced new calibrations, where, RGB slope, tip, and zero point are the functions of abundances. [Tiede et al. 1997], using 4 Galactic open clusters, derived the slope of the RGB - metallicity relation for a younger population, and [Kyeong & Byun 2001] re-derived the calibration, adding 10 new Galactic open clusters. Later on, [Tiede et al 2002] re-examined all existing data used to establish the calibration between the slope of the upper giant branch in a K vs. $J - K$ CMD and the metallicity of the population of stars. They found two very clear linear trends, one for Galactic open clusters spanning $-0.6 < [\text{Fe}/\text{H}] < +0.1$ and another for Galactic globular clusters spanning $-2.2 < [\text{Fe}/\text{H}] < -0.4$. [Valenti et al. 2004] presented new high-quality near-IR photometry of 10 Galactic globular clusters spanning a wide metallicity range ($-2.12 \leq [\text{Fe}/\text{H}] \leq -0.49$). Five of their clusters belong to the Halo and Five to the Bulge. They constructed CMDs in various planes $((K, J - K), (K, V - K), (H, J - H),$ and $(H, V - H))$ and measured a set of photometric indices (colors, magnitudes, and slopes) describing the location and the morphology of the RGB. They combined this new data set with those already published by [Ferraro et al. 2000] and [Valenti et al. 2004a], and presented an updated calibration of the various RGB indices in the

2MASS photometric system regarding the cluster metallicity. Finally, [Kuinskas et al 2008], using a sample of intermediate-age (1-8 Gyr) clusters in the Large and Small Magellanic Clouds, found systematic differences between the RGB slope vs. metallicity relation derived from their sample and that of [Valenti et al. 2004a]. They conclude that this discrepancy cannot be explained in terms of differences in cluster ages, and its origin needs further investigation.

We attempt here to improve the relationship between RGB slope, metallicity and age by adding 23 young, intermediate, and old LMC and SMC clusters.

2 Observations and data reductions

Most observations were obtained over three continuous nights on December 19-21, 2004, with the WFIRC on the 2.5-m du Pont telescope at the Las Campanas observatory (see [Persson et al. 2002] for details). The WFIRC (Wide Field Infrared Camera) dewar houses four Rockwell 1024 x 1024 pixel HgCdTe arrays. The pixel size is 18.5 microns, which gives a scale of 0.196 arcsec/pixel and a linear dimension of 201×201 arcsec for each array at the Cassegrain focus of the 100-inch telescope. The chip No. 2 has the betabnew.dat.smst cosmetics and was used for the observations of the clusters. Chips No. 1,3,4 were used for the background subtraction of the “field” stars.

After the standard reductions of the IR frames, the stellar photometry was carried out with IRAF DAOPHOT II ([see also, Sharma et al. 2020, Sharma et al. 2016]). The final photometry list contains J and K_S magnitudes of 17665 stars with “formal” DAOPHOT errors less than 0.15 mag in each filter. The limiting magnitudes of our photometry are: $J_{\text{lim}} = 18.3 - 19.8$ and $K_{S\text{lim}} = 17.5 - 19.0$. Between 50 and 700 2MASS stars in each field were used to obtain the zero points for transformation to the standard JHK_S system.

The observations of the clusters ESO121-3, NGC 2121, NGC 2249, SL 388, SL 509, SL 817, and SL 862 are presented in this paper were collected with the ESO/NTT telescope at the La Silla observatory in Chile, in the course of the Araucaria project ([Pietrzynski et al. 2006])

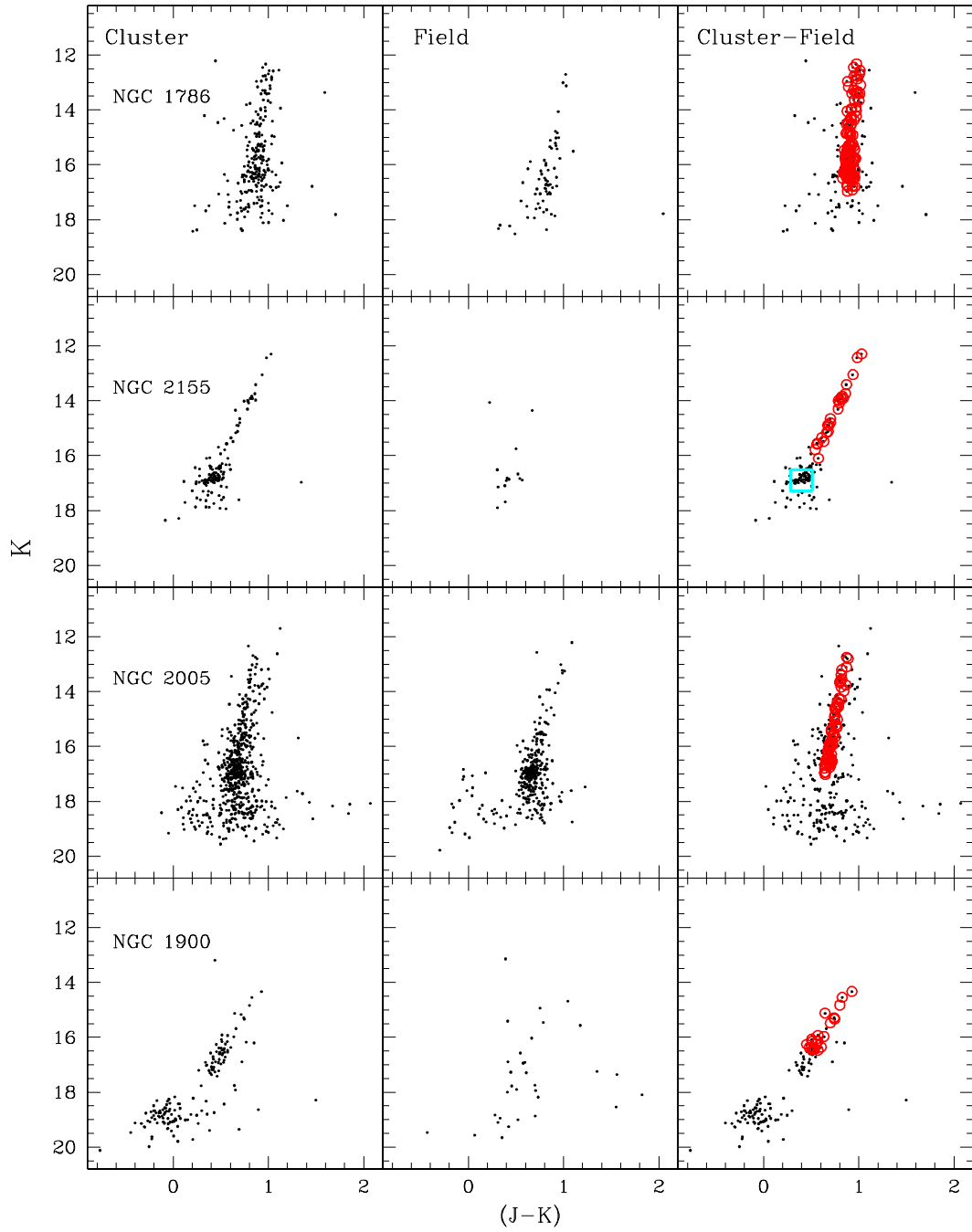


Fig. 1 $(J - K), K$ CMDs for cluster region stars, field region stars, and statistically cleaned cluster member stars. The probable cluster member stars, used to calculate the slope of RGB, are shown in red circles. The location of the horizontal branch for the NGC 2155 cluster is shown with a cyan square box.

Table 1 Cluster ages, metallicities, and RGB slope values.

Cluster	$\alpha_{(2000)}$ ($^{\circ}$)	$\delta_{(2000)}$ ($^{\circ}$)	$[Fe/H]$ (dex)	$\sigma_{[Fe/H]}$	Slope _{RGB}	σ_{Slope}	Log Age	σ_{Age}	Ref Age	Ref [Fe/H]
ESO 121-3*	90.5083	-60.5230	-0.97	0.08	-0.071	0.021	9.417	0.2	1	5
Hodge 2*	79.4542	-69.6440	-0.49	0.07	-0.104	0.011	9.23	0.16	2	6
Hodge 3	83.3321	-68.1520	-0.32	0.05	-0.115	0.006	8.9	0.1	3	7
Kron 28	12.9148	-71.9991	-0.94	0.04	-0.087	0.005	9.57	0.04	4	2
Kron 44	15.5264	-73.9230	-0.78	0.07	-0.09	0.005	9.57	0.08	4	2
Lindsay 1*	0.9750	-73.4720	-0.98	0.07	-0.095	0.004	9.86	0.216	2	4
Lindsay 113*	27.3750	-73.7280	-1.12	0.05	-0.074	0.005	9.56	0.195	2	8
Lindsay 17	8.9238	-73.5976	-0.84	0.03	-0.095	0.009	9.72	0.6	5	9
Lindsay 7	6.1798	-73.7533	-0.76	0.05	-0.09	0.006	9.3	0.27	5	9
NGC 152	8.2365	-73.1157	-0.72	0.06	-0.09	0.005	9.28	0.07	2	2
NGC 1754*	73.5708	-70.4410	-1.45	0.07	-0.08	0.004	10.0	0.1	3	3
NGC 1783	74.7858	-65.9877	-0.54	0.008	-0.104	0.003	9.29	0.09	2	4
NGC 1786*	74.7833	-67.7450	-1.76	0.3	-0.12	0.003	10.06	0.06	3	3
NGC 1795*	74.9417	-69.8010	-0.35	0.04	-0.107	0.008	9.27	0.1	2	10
NGC 1835*	76.2792	-69.4070	-1.69	0.05	-0.091	0.006	10.15	0.05	3	3
NGC 1846*	76.8958	-67.4610	-0.49	0.08	-0.106	0.001	9.29	0.08	2	4
NGC 1898*	79.1708	-69.6570	-1.15	0.05	-0.098	0.005	10.07	0.08	2	3
NGC 1900*	79.7875	-63.0240	-0.55	0.05	-0.12	0.011	8.842	0.01	1	1
NGC 1978	82.1889	-66.2367	-0.49	0.09	-0.097	0.003	9.4	0.12	2	4
NGC 2005*	82.5417	-69.7530	-1.75	0.08	-0.085	0.003	10.12	0.04	2	3
NGC 2019*	82.9833	-70.1590	-1.41	0.06	-0.074	0.004	10.1	0.05	3	3
NGC 2121*	87.0500	-71.4810	-0.54	0.06	-0.087	0.003	9.246	0.23	1	4
NGC 2155*	89.6375	-65.4770	-0.59	0.04	-0.13	0.003	9.45	0.07	2	4
NGC 2210*	92.8792	-69.1210	-1.74	0.11	-0.086	0.003	10.08	0.04	2	3
NGC 2249*	96.4542	-68.9200	-0.45	0.12	-0.091	0.003	9.08	0.1	2	11
NGC 339*	14.4484	-74.4707	-1.15	0.09	-0.093	0.002	9.77	0.17	2	2
NGC 361*	15.5463	-71.6070	-0.9	0.03	-0.103	0.003	9.51	0.1	6	2
NGC 416	16.9960	-72.3557	-0.85	0.08	-0.098	0.005	9.78	0.08	2	2
NGC 419	17.0719	-72.8838	-0.62	0.2	-0.099	0.004	9.3	0.13	2	2
SL 388*	80.0208	-63.4800	-0.39	0.09	-0.067	0.004	9.002	0.12	1	12
SL 509*	82.4500	-63.6490	-0.54	0.05	-0.083	0.004	9.138	0.18	1	1
SL 817*	90.1583	-70.0690	-0.41	0.03	-0.067	0.008	8.877	0.08	1	1
SL 862*	93.3625	-70.6960	-0.47	0.1	-0.078	0.011	8.851	0.09	1	1

*: Observed clusters

Age: 1: [Dhanush et al. 2024] 2: [Milone et. al. 2023] 3: [Narloch et al. 2022] 4: [Gatto et. al. 2021] 5: [Parisi et al. 2022] 6: [Narloch et. al. 2021] [Fe/H]: 1. [Sharma et al. 2010] 2. [Parisi et al. 2022] 3: [Mucciarelli et al. 2021] 4: [Song et al. 2021] 5. [Beasley et al. 2002] 6. [Milone et. al. 2023] 7. [Grocholski et al. 2006] 8. [Da Costa & Hatzidimitroui 1998] 9. [Parisi et al. 2014] 10. [Narloch et al. 2022] 11. [Kerber et al. 2007] 12. [Brocato et al. 2001]

with the main goal is to study the properties of the red clump (RC) stars in the IR domain (e.g. [Pietrzynski et al. 2003]). These clusters were observed with the SOFI instrument in wide-field mode with a focal elongator in the

grism wheel (LFFO) during three different photometric nights together with a large number (typically 6-8 per night) of standard stars from the UKIRT list ([Hawarden et al. 2001]). The resulting field of view was about 2.49×2.49 arcmin square with a scale of 0.146 arcsec/pixel. Since

2005, the LFFO SOFI setup was not offered by ESO. Hence, SOFI observed another three clusters (Lindsay 1, NGC339, Lindsay 113) with a different wide-field mode. In this configuration, the field of view was 4.92×4.92 arcmin square with a scale of 0.288 arcsec/pixel. The total integration times were about 20 and 3 minutes in the K_S and J band filter, respectively. The relatively loose clusters were observed using the so-called simple jittering technique, while in the case of the dense ones, the sky was probed a few arcmin away from the cluster. The PSF photometry was obtained with the DAOPHOT and ALLSTAR programs as described in detail in [Pietrzynski et al. 2002]. The instrumental magnitudes were transformed to the 2MASS photometric system in the same way as for du Pont telescope observations.

3 Result and analysis

3.1 The RGB Slope

The RGB slope is related to the effective temperature of the stars along the RGB, and T_{eff} in turn depends on the opacity and heavy element abundance. This parameter is very powerful because it is independent of reddening and distance. It is significantly less demanding in terms of observing time and telescope collecting area than the spectroscopic methods [Ivanov & Borissova 2002]. [Ivanov & Borissova 2002] and [Kuchinski & Frogel 1995] argued that the RGB morphology can be very well constrained through the RGB slope, which is linearly fitted between 0.6 and 5.1 mag brighter than the zero-age horizontal branch (ZAHB). However, [Valenti et al. 2004a] argued that in the case of low-intermediate-metallicity clusters, the accurate measurement of the location of the ZAHB in IR CMD is impossible because the HB is not horizontal at all. To apply a homogeneous procedure to the entire cluster sample, they fit the RGB in the magnitude range between 0.5 and 5 mags fainter than the brightest star of each cluster after previous decontamination by the asymptotic giant branch and field stars. Also, [Kuinskas et al 2008] studied 14 LMC/SMC clusters and derived RGB slopes using the slightly different criteria, using RGB stars in the range $M_{K_s} = -2.0$ to -6.4 for fitting. [Kyeong & Byun 2001] in their study of RGB slopes from old open Galactic clusters, include

those stars in the giant branch only with absolute magnitude in the range $-1.5 \leq M_K \leq -6.5$. This criteria is similar to [Tiede et al. 1997]’s approach. This criterion excludes both RC stars and bright asymptotic giant branch stars.

In this study, we followed the procedure to determine the RGB slope described in [Ivanov & Borissova 2002], carrying out a least-squares fit to the RGB from 0.5 mag above the horizontal branch (cf. Fig. 1) using the equation:

$$(J - K_S) = ZP + \text{Slope}_{\text{RGB}} \times K_S \quad (1)$$

on the statistically cleaned CMD to derive the slope and the zero point, assuming K_S to be the independent variable. The LMC and SMC are relatively nearby targets, and the globular clusters span a wide range of metallicity and age. From 23 clusters of our sample, there are 4 SMC clusters (Lindsay 1, Lindsay 113, NGC 339, 361) and the rest 19 belong to LMC. From our photometry, we got good quality NIR data (error < 0.1 for $K=18$ mag), and it has been used to generate CMDs for all the target clusters. Cluster membership criteria is crucial in defining the cluster parameters. As we can’t reach the faint limits of our NIR observation through Gaia’s proper motion data, we statistically subtracted the contribution of field stars from the CMD of the cluster region following the approach of [Sharma et al. 2017]. The CMD of the cluster and field region were divided into rectangular bins of size 0.5 in K_S mag and 0.25 mag in $J - K_S$ color. Then, from each bin of the cluster CMD, we randomly removed a number of stars equal to the number of stars in the corresponding bin of the “field” CMD. We have defined the cluster region as a circular area corresponding to the angular dimension of the cluster where the stellar density reaches the background density. The cluster centers and radii are chosen by eye, based primarily on the photometric catalog. We have used a circular annulus around the cluster having the same area as the cluster region for a field star distribution. Fig. 1 shows K , $(J - K)$ some examples of CMDs for the stars in clusters regions (left panels) and corresponding field regions (middle panels). We show clusters with different ages and metallicities. The contamination due to background field population is visible in the cluster region CMDs, which, in some cases, is ~ 40 -50% of the stars in the designated cluster area. In

most of the older clusters, these two populations are almost completely overlaid and only precise statistical analysis can distinguish them. The statistically cleaned K , $(J - K)$ CMD of the cluster region is also shown in the right panels of Fig. 1, clearly showing the distribution of RGB stars in the clusters. The RGB locus was then defined after inspecting each CMD. We removed $10\text{-}\sigma$ outliers, and repeated the fitting. Typically, the fitting coefficients obtained after two iterations were statistically indistinguishable. The probable cluster member stars, which are used to calculate the slope of RGB, are shown in red circles in Fig. 1 for a few sample clusters. A total of 300 realizations were generated using Monte Carlo simulations for each cluster – each including the contamination removal and the fitting – and we averaged the fitting results (see also [Ivanov & Borissova 2002] and [Ivanov et al. 2000]). The derived value of the slope of the RGB stars of the clusters is given in Table 1.

For four clusters in our sample, namely NGC 1900, NGC 2155, NGC 2005 and NGC 1788 we noticed some discrepancy of the derived RGB slopes from the main trend of the rest of the clusters. We performed additional checks to validate the slope value (or not). Using the VISTA Science Archive (VSA, <http://vsa.roe.ac.uk/index.html>), we retrieved the merged J and Ks photometric catalogs (5×5 arcmin square field around the center of each cluster) from Vista Magellanic Cloud NIR survey (VMC, [Cioni et al. 2011]). Then, the stars are cross-matched with the Gaia EDR3 proper motion and photometry catalog ([Gaia Collaboration 2016]). In addition to the statistical cleaning used above, the most probable cluster members are verified by the combination of proper motions and VMC Ks , $(J - Ks)$ color-magnitude diagrams. The process is illustrated in Fig. 2, and we got similar RGB slope values.

3.2 RGB slope-metallicity-age calibration

A sample of star clusters is constructed as follows: for LMC and SMC, we used our data presented in this paper plus [Kuinskas et al 2008] sample transformed to our RGB slope estimation. The ages of the LMC and SMC clusters are taken from the literature, using mainly two recent works [Dhanush et al. 2024] and [Narloch et al. 2022], to

maintain the homogeneity. They are listed in the Table 1 with the corresponding references. Our sample contains both young and old clusters, the youngest cluster in the sample is NGC 1900, with an age of 700 Myr, and the oldest one NGC 2005 has an age of around 13 Gyr. The metallicities of the clusters in our sample are based on the latest and most reliable measurements in the literature. They are also listed in Table 1 with the corresponding references.

As a consistency check of the homogeneity of the age and metallicities taken from the literature of such constructed star cluster sample, we plotted the well-known Age-metallicity relation (AMR) in the right panel of Fig. 3. The red circles represent SMC clusters, and the blue circles represent the LMC sample. In the left panel, we compare the AMR relation for the LMC and SMC clusters sample taken from [Narloch et al. 2022], their Fig.13.

The LMC sample follows the bursting models of [Pagel & Tautvaisiene 1998], with the age gap between 3 and 10 Gyr. The low-metallicity clusters are situated before the age gap, while the most metal-rich clusters have been formed recently ([for more details, see Sharma et al. 2010]). The SMC clusters are too few to make any conclusion.

The next relation we build in our analysis is the $\log(\text{Age})$ - RGB slope for all clusters in our sample, shown in Fig. 4. As seen from the plot, there are no shifts in the location on the diagram of the LMC and SMC clusters; therefore, they can be used as homogeneous samples. The RGB slope do not shows any statistically significant age dependence. The correlation coefficient of both groups (LMC and SMC) is around 0.05.

And finally, we have plotted the RGB slope as a function of $[\text{Fe}/\text{H}]$ for all clusters in our sample (Fig. 5). Magenta circles represent the whole sample, the black ones for clusters younger than 3 Gyr, and the grey circles stand for clusters older than 10 Gyr.

The least-square fit to the whole sample is:

$$[\text{Fe}/\text{H}] = -4.13_{\pm 1.2} \times \text{Slope}_{\text{JK}}^{\text{RGB}} - 1.24_{\pm 0.5} \quad (2)$$

The least-square fit to the clusters older than 10 Gyr is:

$$[\text{Fe}/\text{H}] = 2.64_{\pm 0.9} \times \text{Slope}_{\text{JK}}^{\text{RGB}} - 1.33_{\pm 0.22} \quad (3)$$

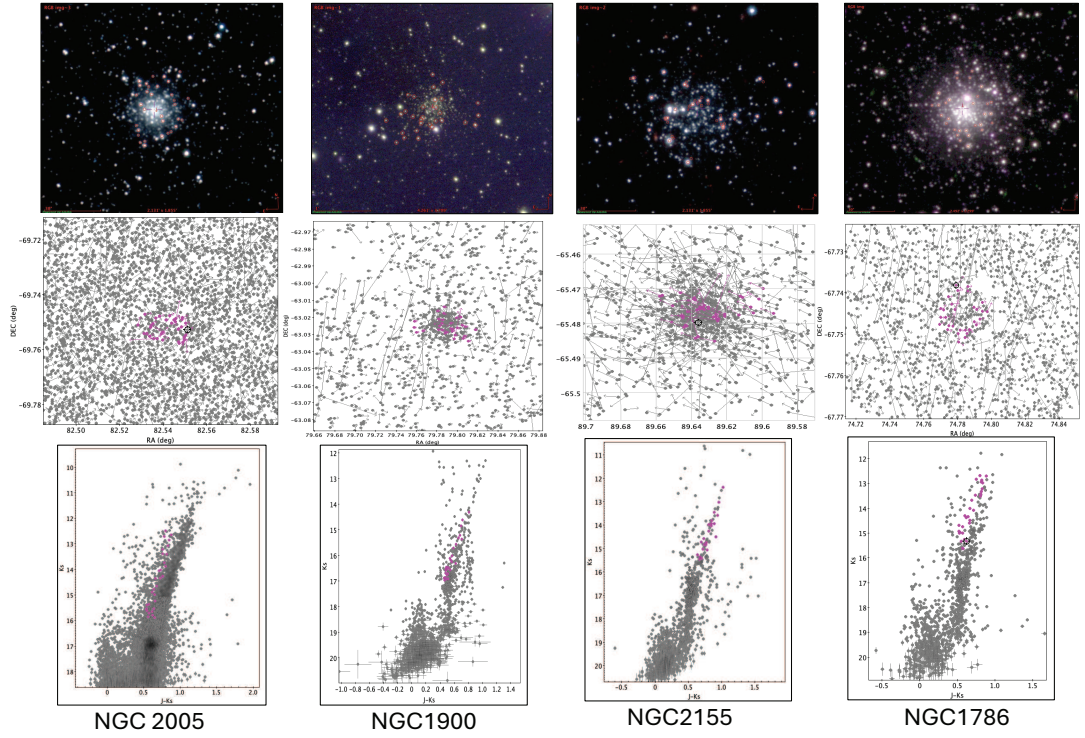


Fig. 2 The false color Y , J and K images, proper motion diagrams and color-magnitude diagrams of NGC 1900, NGC 2155, NGC 2005 and NGC 1788. The images are taken from the VISTA Magellanic Cloud survey. The black dots are all stars in the 5×5 arcmin square field around the center of each cluster. The most probable RGB members used to derive the RGB slope are marked with red circles.

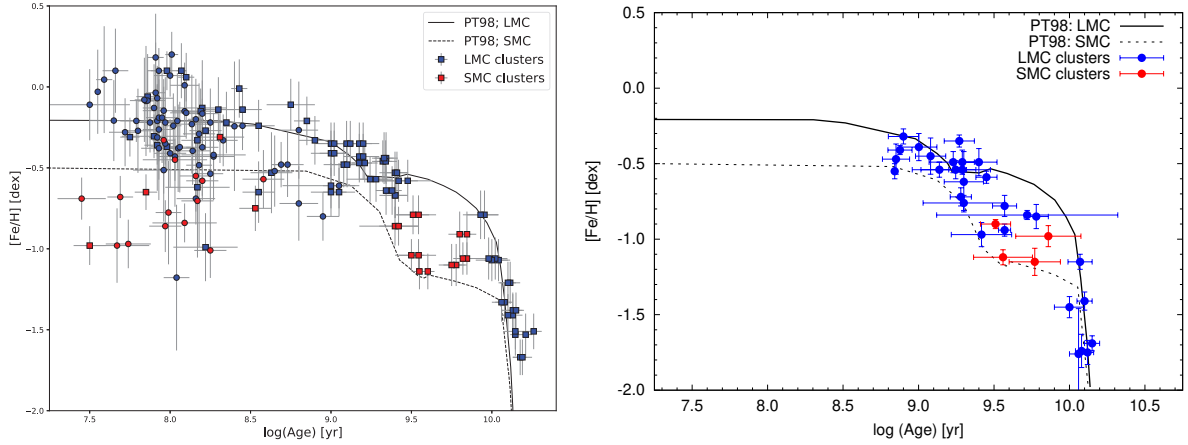


Fig. 3 Left panel: $\text{Log}(\text{Age})$ vs. $[\text{Fe}/\text{H}]$ (AMR) relation for the LMC and SMC clusters sample taken from [Narloch et al. 2022], their Fig.13. Right panel: $\text{Log}(\text{Age})$ vs. $[\text{Fe}/\text{H}]$ (AMR) relation for the present LMC and SMC clusters sample. Blue circles represent LMC clusters, and the red circles represent the SMC sample. The solid and dashed lines correspond to LMC and SMC from the bursting models of [Pagel & Tautvaišienė 1998].

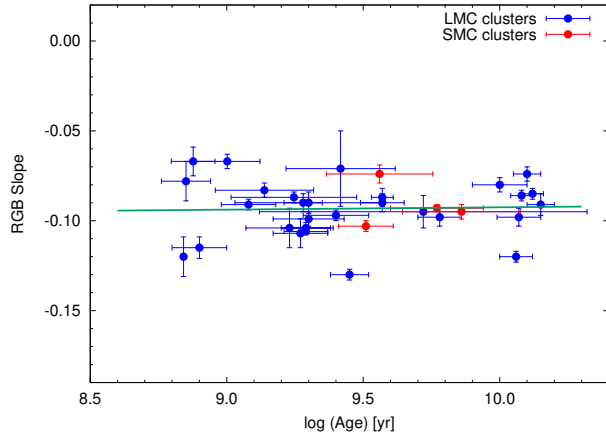


Fig. 4 The Log (Age) vs. RGB slope relation for the clusters from our sample. The symbols are the same as in Fig. 3. The solid line is the least square fit to the whole cluster sample.

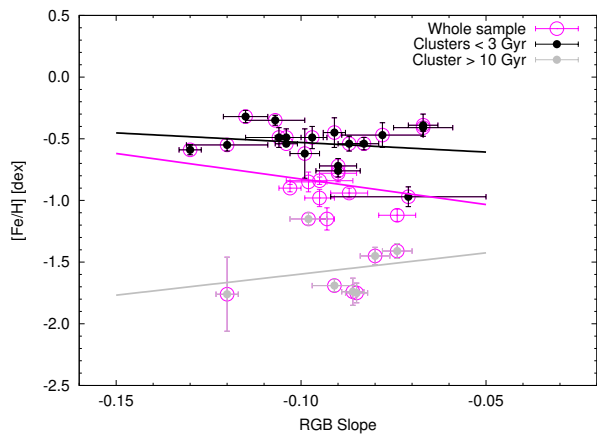


Fig. 5 The RGB slope vs. [Fe/H] relation. The black circles represent the clusters younger than 3 Gyr, and the grey ones represent clusters older than 10 Gyr. Magenta circles represent the whole cluster sample. The solid lines represent the derived best fit for the corresponding sample.

The least-square fit to the clusters younger than 3 Gyr is:

$$[\text{Fe}/\text{H}] = -1.55_{\pm 0.5} \times \text{Slope}_{\text{JK}}^{\text{RGB}} - 0.69_{\pm 0.8} \quad (4)$$

The conservative uncertainty of the individual photometric cluster metallicity estimate, due to uncertainties in the cluster slope derivation, age, metallicity, etc., can be estimated as 0.3 dex.

As can be seen, the young clusters do not show statistically significant RGB slope [Fe/H] dependence, and some weak relations can be found for the older clusters.

4 Conclusions

This paper presents deep near-IR *JHK* stellar photometry for 23 LMC/SMC globular clusters. SOFI and Du-pont images enable us to go as deep as 18 mags in the K band; therefore, for the majority of the clusters, the $J - K_S, K_S$ CMDs reveal well-defined RGBs. The well-defined RGBs of the cluster have been used to determine their slopes which in turn are used to determine the relation between slope-age-metallicity. We checked the AMR for the present sample and found LMC clusters follow the burst model of [Pagel et al. 1999], with an age gap between 3-10 Gyr. The RGB slope of the present LMC/SMC cluster sample does not show any statistically significant age dependence. We have checked the dependence of the RGB slope on the metallicity for all 33 LMC/SMC clusters in the present sample. They follow the prediction of the theoretical models. The young and old clusters are found to be distributed differently in RGB slope-metallicity space. The population of the younger clusters shows a marginal negative slope, whereas the older clusters show a positive slope.

Acknowledgements. The data used in this paper have been obtained with du Pont telescope at Las Campanas observatory and ESO NTT at La Silla observatory. Support for SS and JB are also provided by ANID's Millennium Science Initiative ICN12-009, awarded to the Millennium Institute of Astrophysics (MAS).

Declarations

- Data availability: Fig.1: Available on request. Fig 2, Fig 3, Fig 4: Available in Table 1.

References

- [Beasley et al. 2002] Beasley, M. A., Hoyle, F., Sharples, R. M. 2002, MNRAS, 336, 168
- [Brocato et al. 2001] Brocato, E., Di Carlo, E., Menna, G. 2001, A&A, 374, 523

- [Cioni et. al. 2011] Cioni, M. -R. L., Clementini, G., Girardi, L. et. al. 2011, *A&A*, 52, A116
- [Dhanush et al. 2024] Dhanush, S. R., Subramaniam, A., Nayak, P. K., Subramanian, S. 2024, *MNRAS*, 528 2274
- [Da Costa & Hatzidimitroui 1998] Da Costa, G., Hatzidimitrou, D. 1998, *AJ*, 115, 1934
- [Ferraro et al. 2000] Ferraro, F., Montegriffo, P., Origlia, L., Fusi Pecci, F. 2000, *AJ*, 119, 1282
- [Gaia Collaboration 2016] Gaia Collaboration, 2016, *A&A*, 595, 1
- [Gatto et. al. 2021] Gatto, M., Ripepi, V., Bellazzini, M. et. al. 2021, *MNRAS*, 507, 3321
- [Grocholski et al. 2006] Grocholski, A. J., Cole, A. A., Sarajedini, A., Geisler, D., Smith, V. V. 2006, *AJ*, 132, 1630
- [Hawarden et al. 2001] Hawarden, T., Leggett, S., Letawsky, M., Ballantyne, D., Casali, M. 2001, *MNRAS*, 325, 563
- [Ivanov & Borissova 2002] Ivanov, V.D., Borissova, J. 2002, *A&A*, 390, 937
- [Ivanov et al. 2000] Ivanov, V.D., Borissova, J., Alonso-Herrero, A., Russeva, T. 2000, *ApJ*, 119, 2274
- [Kerber et al. 2007] Kerber, L. O., Santiago, B. X., Brocato, E. 2007, *A&A*, 462, 139
- [Kuchinski et al. 1995] Kuchinski L., Frogel, J., Terndrup, D., Persson, S. 1995, *AJ*, 109, 1131
- [Kuchinski & Frogel 1995] Kuchinski, L., Frogel, J. A. 1995, *AJ*, 110, 2844
- [Kuinskas et al 2008] Kuinskas, A., Dobrovolskas, V., Cerniauskas, A., Tanab, T. 2008, *Baltic Astronomy*, 17, 363
- [Kyeong & Byun 2001] Kyeong, J., Byun, Y. 2001, *JKAS*, 34, 137
- [Narloch et. al. 2021] Narloch, W., Pietrzyński, G., Gieren, W. et. al. 2021, *A&A*, 647, 135
- [Milone et. al. 2023] Milone, A. P., Cordoni, G., Marino, A. F. et. al. 2023, *A&A*, 672, 161
- [Minniti et al. 1995] Minniti, D., Olszewski, E., Rieke, M. 1995, *AJ*, 110, 1686
- [Mucciarelli et al. 2021] Mucciarelli, A., Massari, D., Minelli, A., Romano, D., Bellazzini, M., Ferraro, F. R., Matteucci, Origlia, L. 2021, *NatAs*, 5, 1247
- [Narloch et al. 2022] Narloch, W., Pietrzyński, G., Gieren, W., et al., 2022, *A&A*, 666A, 80
- [Pagel & Tautvaisiene 1998] Pagel, B. E. J., Tautvaisiene, G. 1998, *MNRAS*, 299, 235
- [Pagel et al. 1999] Pagel, B. E. J., Tautvaisiene, G. 1999, *Ap&SS*, 265, 461
- [Parisi et al. 2014] Parisi, M. C., Geisler, D., Carraro, G., Clariá, J. J., Costa, E., Grocholski, A. J., Sarajedini, A., Leiton, R., Piatti, A. E. 2014, *AJ*, 147, 71
- [Parisi et al. 2022] Parisi, M. C., Gramajo, L. V., Geisler, D., Dias, B., Clariá, J. J., Da Costa, G., Grebel, E. K 2022, *A&A*, 662, 75
- [Persson et al. 2002] Persson, S., Murphy, D., Gunnels, S., Birk, C., Bagish, A., Koch, E. 2002, *AJ*, 124, 619
- [Pietrzyński et al. 2002] Pietrzyński, G., Gieren, W. 2002, *AJ*, 124, 2633
- [Pietrzyński et al. 2006] Pietrzyński, G., Gieren, W. 2006, *MmSAI*, 77, 239
- [Pietrzyński et al. 2003] Pietrzyński, G., Gieren, W., Udalski, A. 2003, *AJ*, 125, 2494
- [Saviane et al. 2000] Saviane, I., Rosenberg, A., Piotto, G., Aparicio, A. 2000, *A&A*, 355, 966
- [Sharma et al. 2010] Sharma, S., Borissova, J., Kurtev, R., Ivanov, V. D., Geisler, D. 2010, *AJ*, 139, 878

- [Sharma et al. 2020] Sharma, Saurabh, Ghosh, A., Ojha, D. K., Pandey, R., Sinha, T., Pandey, A. K., Ghosh, S. K., Panwar, N., Pandey, S. B. 2020, MNRAS, 498, 2309
- [Sharma et al. 2017] Sharma, Saurabh, Pandey, A. K., Ojha, D. K., Bhatt, H., Ogura, K., Kobayashi, N., Yadav, R., Pandey, J. C. 2017, MNRAS, 467, 2343
- [Sharma et al. 2016] Sharma, Saurabh, Pandey, A. K., Borissova, J., Ojha, D. K., Ivanov, V. D., Ogura, K., Kobayashi, N., Kurtev, R., Gopinathan, M., Kesh Yadav, R., 2016, AJ, 151, 126
- [Song et al. 2021] Song, Y., Mateo, M., Bailey, J. I., Walker, M. G., Roederer, I. U., Olszewski, E. W., Reiter, M., Kremin, A. 2021, MNRAS, 504, 4160
- [Spergel et al. 2007] Spergel et al. 2007, ApJS, 170, 377
- [Tiede et al. 1997] Tiede, G., Martini, P., Frogel, J. 1997, AJ, 114, 694
- [Tiede et al 2002] Tiede, G., Sarajedini, A., LaVine, J. 2002, AAS, 201. 709
- [Valenti et al. 2004a] Valenti, E., Ferraro, F. R., Perina, S., Origlia, L. 2004a, A&A, 419, 139
- [Valenti et al. 2004] Valenti, Ferraro, F., Origlia, L. 2004, MNRAS, 351, 1204